An auroral scintillation observation using precise, collocated GPS receivers

T. W. Garner,[1] R. B. Harris,[1] J. A. York,[1] C. S. Herbster,[2] C. F. Minter III,[2] and D. L. Hampton[3]

Received 6 April 2010; revised 17 November 2010; accepted 21 December 2010; published 26 February 2011.

[1] On 10 January 2009, an unusual ionospheric scintillation event was observed by a Global Positioning System (GPS) receiver station in Fairbanks, Alaska. The receiver station is part of the National Geospatial-Intelligence Agency's (NGA) Monitoring Station Network (MSN). Each MSN station runs two identical geodetic-grade, dual-frequency, full-code tracking GPS receivers that share a common antenna. At the Fairbanks station, a third separate receiver with a separate antenna is located nearby. During the 10 January event, ionospheric conditions caused two of the receivers to loose lock on a single satellite. The third receiver tracked through the scintillation. The region of scintillation was collocated with an auroral arc and a slant total electron content (TEC) increase of 5.71 TECu (TECu = 10^{16}/m^2). The response of the full-code tracking receivers to the scintillation is intriguing. One of these receivers lost lock, but the other receiver did not. This fact argues that a receiver's internal state dictates its reaction to scintillation. Additionally, the scintillation only affected the L2 signal. While this causes the L1 signal to be lost on the semicodelessly receiver, the full-code tracking receiver only lost the L1 signal when the receiver attempted to reacquire the satellite link.

Citation: Garner, T. W., R. B. Harris, J. A. York, C. S. Herbster, C. F. Minter III, and D. L. Hampton (2011), An auroral scintillation observation using precise, collocated GPS receivers, *Radio Sci.*, *46*, RS1018, doi:10.1029/2010RS004412.

1. Introduction

[2] Global Navigation Satellite Systems (GNSS) like the Global Positioning System (GPS) transmit navigation signals at ultrahigh frequencies (UHF) to Earth from a constellation of orbiting satellites. These electromagnetic waves pass through the ionosphere and plasmasphere, which can alter radio waves. GNSS signals are delayed and refracted by the plasma's index of refraction and its variation [*Davies*, 1990]. This refraction is frequency dependent, and GNSS systems transmit the same signal on two or more separate frequencies to remove ionospheric time delays. In addition, the phase, amplitude, angle of arrival, and polarization of the GNSS waves can vary as the wave travels through irregularities within the plasma [*Yeh and Liu*, 1982; *Kintner et al.*, 2007]. Such variations are called scintillation, and are caused by medium (few kilometers) to small (few centimeter) scale irregularities. It is more difficult to engineer a system that tracks through ionospheric scintillation than to create a system that removes ionospheric time delay. This is why ionospheric scintillation remains a major space weather challenge to satellite navigation and communication systems.

[3] Ionospheric scintillation has been observed at all latitudes and in all geomagnetic conditions [e.g., *Aarons*, 1982; *Coster et al.*, 2005]. However, scintillation is most common in the equatorial ionosphere shortly after the prereversal enhancement [e.g., *Basu and Basu*, 1981; *Basu et al.*, 1996; *Fejer et al.*, 1999; *Su et al.*, 2008]. Scintillation also frequently occurs in the auroral oval and polar cap [e.g., *Aarons*, 1982; *Tsunoda*, 1988; *Kintner et al.*, 2007]. High-latitude scintillations was observed in the UHF and VHF frequency bands before the advent of GPS [e.g., *Basu*, 1975; *Martin and Aarons*, 1977; *Rino and Matthews*, 1980; *Basu and Aarons*, 1980] and since [e.g., *Pryse et al.*, 1996; *Coker et al.*, 2004]. In the GPS era, several studies [e.g., *Doherty et al.*, 2003; *Forte and Radicella*, 2002; *Kintner et al.*, 2002; *Forte*, 2008; *Smith et al.*, 2008; *Jayachandran et al.*, 2009] have used GPS signals to study the auroral oval and polar ionosphere and

[1]Space and Geophysics Laboratory, Applied Research Laboratories, University of Texas at Austin, Austin, Texas, USA.
[2]National Geospatial-Intelligence Agency, Arnold, Missouri, USA.
[3]Geophysical Institute, University of Alaska Fairbanks, Fairbanks, Alaska, USA.

0048-6604/11/2010RS004412

the plasma irregularities associated with scintillation. Because of their higher frequencies, GPS signals are less susceptible to scintillation, and scintillation of GPS signals at midlatitudes only occurs during large magnetic storms. These studies have used civilian grade receivers that track the GPS signals either codelessly or semicodelessly [*Kintner et al.*, 2007].

[4] Much of the basic morphology and physics of auroral scintillation has been uncovered. From an operational point of view, the most significant discovery is that high-latitude scintillation tends to be observed in the phase [*Nichols et al.*, 2000; *Doherty et al.*, 2003]. The amplitude does respond, but is less common. In terms of the receiver response, scintillation is observed in the amplitude if the plasma variations are faster than the receiver's integration time and in the phase if the plasma variations are slower than the integration time. Additionally, the spectra of the high-latitude plasma irregularities typically obey a power law distribution [*Yeh and Liu*, 1982]. These distributions correspond to the predictions of weak scattering phase screen theory [*Rino*, 1979]. While much has been learned about auroral scintillation, there is still a significant amount to understand, especially with regard to how the complex tracking loops used by GNSS receivers react to ionospheric scintillation.

[5] This paper presents recent observations of ionospheric scintillation observed by three collocated GPS receivers in Fairbanks, Alaska. The scintillation occurred when a bright auroral arc was within the receivers' line of sight. The L2 channel (1.2276 GHz, 24.42 cm) was strongly impacted causing two receivers to lose lock on the signal. One of these receivers was tracking the full code; the other was tracking semicodelessly. A full-code tracking receiver is one that uses an encryption key to track the P code. Because the third receiver tracked through the scintillation, it was able to measure the slant total electron content (TEC) and phase changes associated with the scintillation.

[6] These measurements provide new insight into a GPS receiver's response to scintillation. Two of the three receivers used in this study track the full GPS code. They also share a common antenna. However, these receivers of the same make and model and sharing a common antenna reacted differently to the scintillation event. One receiver lost lock, while the other receiver tracked through the scintillation. These results indicate that a GPS receiver's internal state strongly determine the receiver's reaction to ionospheric scintillation. This implies that while the new civilian GPS codes may help receivers track through ionospheric scintillation, they are unlikely to provide a complete solution to the problem.

2. Monitoring Station Network

[7] The National Geospatial-Intelligence Agency (NGA) maintains a global network of geodetic quality, dual-frequency, full-code tracking GPS monitoring stations called the Monitoring Station Network [*Creel et al.*, 2007]. There are 13 active Monitoring Station Network (MSN) station including one test station located in Austin, Texas. Each station consists of two Ashtech Z(Y)-12 dual-frequency receivers with separate cesium clock standards. The cesium clock standards provide each receiver long-term clock stability. Because of the increased clock stability, the phase lock loops (PLLs) within each receiver does not have to compensate for as much clock wander as on a receiver without an external clock standard. Each station's receivers are connected to a common antenna. To mitigate ground multipath noise, the antenna is protected by a choke ring. Additionally, the antenna is covered by a ray dome. Each MSN receiver takes pseudorange and carrier phase observations every 1.5 s and sends the data in real time to the NGA GPS Monitor Station Network Control Center in St. Louis.

[8] *Groves et al.* [2000] compared the performance of several GPS receivers including Ashtech Z-12 receivers during strong scintillation conditions and found that Ashtech receivers tracked well during scintillation. However, the internal Ashtech position solutions were inaccurate because the receivers calculated their position solutions using all of the satellites in view including those experiencing the scintillation. The MSN system is not affected by the problems presented by *Groves et al.* since the receiver's position solution is not used. The external clock standards reduces the need for on-the-fly station clock calculation (a product of the receiver position solution) and the network is only providing the pseudorange and carrier phase observations.

[9] This study focuses upon observations from the Alaskan MSN station, which is located in Fairbanks, Alaska (212.89°E, 64.54°N). Because of its proximity to the auroral oval, this station experiences more signal interruptions than other MSN stations. To better understand the causes of these interruptions, this station has been augmented with a third Ashtech receiver on a separate antenna located 62 cm away from the primary antenna. The third receiver uses Ashtech's semicodeless Z mode tracking instead of full-code tracking by normal MSN receivers and does not have a cesium clock standard.

3. Observations

3.1. Period of Observed Scintillation Events

[10] A short scintillation event occurred on 10 January 2009 between 0923:09 and 0925:01.5 UT. Two of the three receivers at Fairbanks, Alaska, station lost lock to one of the GPS satellite during this period. The other receiver tracked through the scintillation event. The lost signal was to the satellite designated PRN 3. GPS satellites

are designated by one of the 32 pseudorandom noise (PRN) codes, which they broadcast.

[11] This event occurred during quiet geomagnetic conditions (Kp = 1, provisional AE = 156.5 nT). However, an auroral arc was observed in the receiver's field of view during this time period. Figure 1 presents airglow observations of this arc. Figure 1 (top) is an image from the digital, white light all-sky imager at Poker Flat. It was projected onto a geographic map. Figure 1 (bottom) is a keogram from the Poker Flat meridian scanning photometer. Poker Flat is roughly 50 km northeast of Fairbanks. This all-sky image was taken at 0923 UT, and the geographic projection placed at 100 km. The auroral arc was clearly visible, even though the moon polluted the southern portion of the image. Figure 1 (bottom) is a time history of the intensities (in rayleighs) of three different airglow lines from 0900 to 1000 UT. These three airglow lines correspond to 557.7 nm (oxygen green line), 427.8 nm (N_2^+ blue line) and 630.0 nm (oxygen red line). The green and blue lines are emitted in the E region (~100 km) of the ionosphere, while the red line is emitted in the F region (~250–300 km). Figure 1 (bottom), bright auroral arcs were visible at 0922–0924 UT, 0936–0938 UT, and 0946–0948 UT. The large bright red light region between 120° and 140° was caused by moonlight contamination. The scintillation occurred at 0923:09 UT, which was collocated with the first auroral arc. The red to blue ratio of this arc was from 0.2 to 0.4, which corresponds to a characteristic energy for precipitating electrons of 2.5 to 4 keV [*Rees and Luckey*, 1974]. At these energies, the precipitating particle will generate significant ionization in the E region. Similarly, the brightening of the green and blue lines indicated an enhancement of the E region plasma density. The red line brightening was related to an increase in the F region density. However, the red line brightening over the background was smaller than the corresponding blue and green line brightenings. This suggests that any TEC increase over the background collocated with the arc was mostly an E region density increase.

3.2. Carrier-to-Noise Density Observations

[12] The MSN receivers return the carrier-to-noise density ratio (C/No) in dB Hz for each channel. The C/No values are the best available measurement of the incoming signal amplitudes. However, the reported C/No values at a 0.667 Hz data rate are those after the signal correlator, and do not properly represent the signal power at the antenna. Because receivers 1 and 2 share a common antenna, their signal strength from the antenna is equal. However, the internal state of each receiver, different line losses on the antenna cables and their internal noise floors can produce different C/No values after the correlator. In addition, both phase and amplitude scintillation change the postcorrelator C/No since both forms of scintillation alter the incoming waveform. Since suitable high cadence (on the order of mHz) C/No values were not available, neither the S2 nor S4 index was calculated. However, the low-cadence C/No values do provide insight into the signal's behavior as it passes through the disturbed ionosphere.

[13] Figure 2 presents the C/No values for all three channels on each receiver for the period between 0920 and 0930 UT. In Figure 2, the C/A C/Nos are represented as black pluses, the L1 C/Nos are shown as green squares, and the L2 C/No values are represented as blue dots. The Ashtech receivers measure the C/No in units of 0.35 dB Hz. They also have a natural jitter in the C/No between values 0.35 dB Hz. Because receiver 3 tracks the signal's semicodelessly, its C/No values are ~13 dB Hz less than the C/No of the full-code tracking receivers.

[14] The C/No values show the receivers' reactions to the scintillation. At 0920:00 UT, the C/No values for all channels on all receivers behaved normally. Receiver 1 experienced a 2.44 dB Hz loss on the L2 channel at 0923:07.5 UT before losing lock at 0923:09 UT. The receiver attempted to correlate the L2 code until 0924:37.5 UT. During this period, the receiver continued to track the L1 code. At 0924:40.5 UT, the receiver quit tracking PRN 3 until it reacquired the satellite at 0925:01.5 UT. By 0926:10.5 UT, the receiver resumed full-code tracking. Receiver 2 suffered a 2.43 dB Hz loss on L2 at 0923:07.5 UT. The L2 C/No dropped a total of 4.52 dB Hz before reaching a minimum at 0923:10.5 UT. The L2 channel on receiver 2 made a full recovery by 0923:21 UT. The L1 channel was not affected. The semicodeless receiver behaved differently. The L2 channel experienced an initial drop at 0923:06 UT and fluctuated around this level until 0923:28.5 UT when the C/No dropped out before attempting to reacquire. The semicodeless L1 C/No began to slowly decrease starting at 0923:06 UT and stopped at 0924:51 UT when the C/No reaches 0 dB Hz. Receiver 3 reacquired PRN 3 at 0925:03 UT. The C/A C/No values remained constant for all three receivers throughout this period. These observations demonstrate that the scintillation event only disrupted the L2 correlator.

Figure 1. The observed auroral airglow during the scintillation event. (top) An all-sky image from the digital imager taken at 0923 UT, showing an auroral arc in the MSN stations field of view. (bottom) The intensity (in rayleighs) of three different airglow lines observed by the meridian scanning photometer. The green, blue, and red lines show enhancements coincident with an auroral arc.

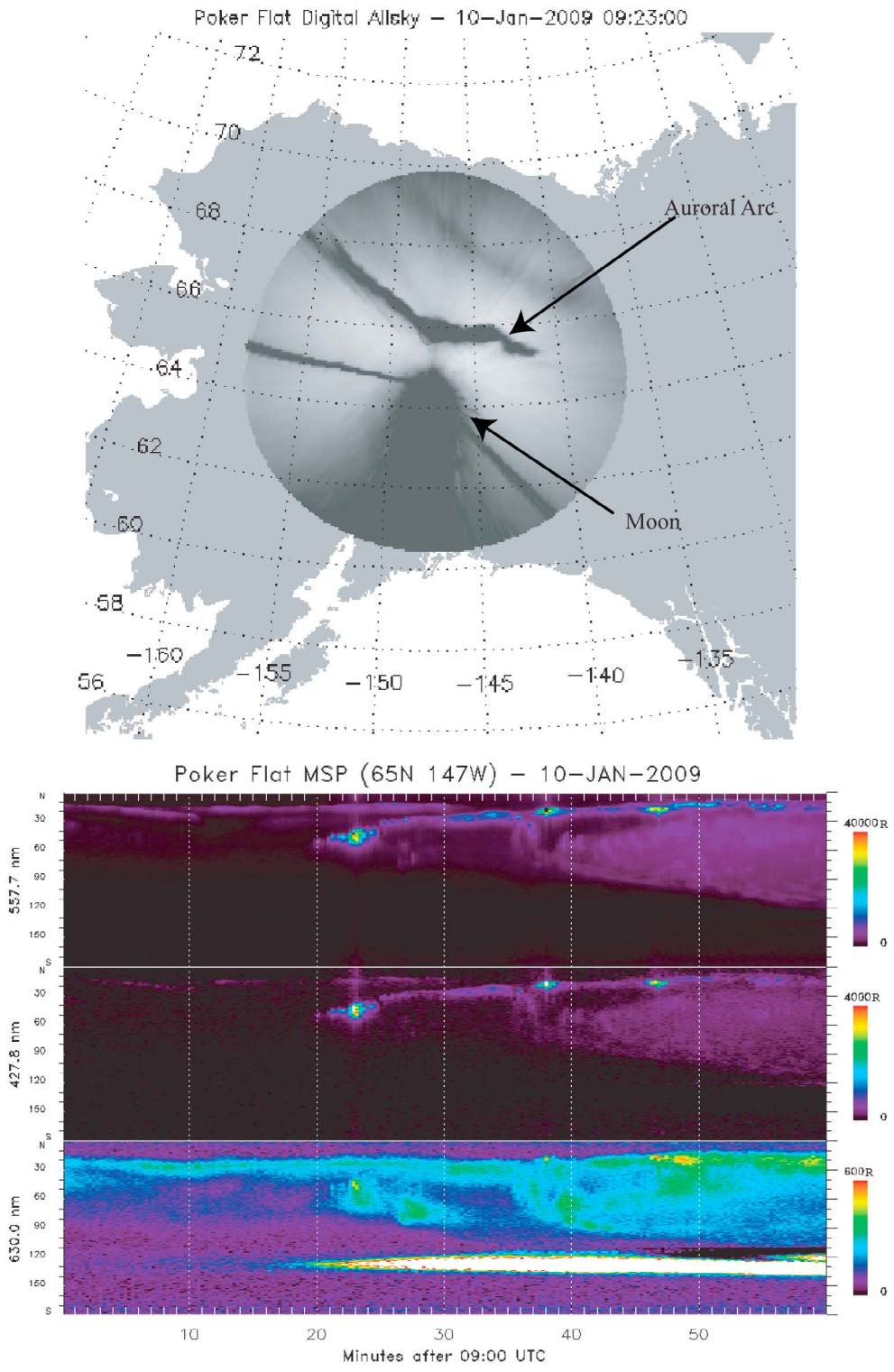
Poker Flat Digital Allsky – 10–Jan–2009 09:23:00
72
70
68
66
64
62
60
58
56
–160
–155
–150
–145
–140
–135
Auroral Arc
Moon
Poker Flat MSP (65N 147W) – 10–JAN–2009
557.7 nm
427.8 nm
630.0 nm
40000R
0
4000R
0
600R
0
10
20
30
40
50
Minutes after 09:00 UTC

Figure 1

3.3. Phase Variations

[15] The raw phase measurements are dominated by the satellite's motion and an unknown phase ambiguity, which hide the impact of the ionosphere on the phase. Typically, GPS phase measurements are detrended by passing the phase measurements through a high-pass filter to remove noise and the effects of the satellite motion [e.g., *Forte and Radicella*, 2002; *Kintner et al.*, 2007]. In this study, the phases observed by receiver 2 were passed through a sixth-order high-pass Butterworth filter and its conjugate with a 0.1 Hz cutoff frequency. The resultant phase variations are shown in Figure 3. Here, the L1 phase variations are shown as pluses and the L2 values as squares. The C/A phase variations are not presented because they mirror the L1 phase variations but with a 15 second time shift.

[16] During this event, the phase variations began a significant increase at 0922:51 UT and continued to 0924:09 UT. The phase variations occurred in both signals but were greater in the L2 channel. At 0923:09 UT, the L2 phase variation was 0.724 cycles below the nominal phase, coincident with the sample time at which receiver 1 lost lock. After 0924:09 UT, the phase variations returned to the zero baseline, which indicate that a cycle slip was not induced by the scintillation.

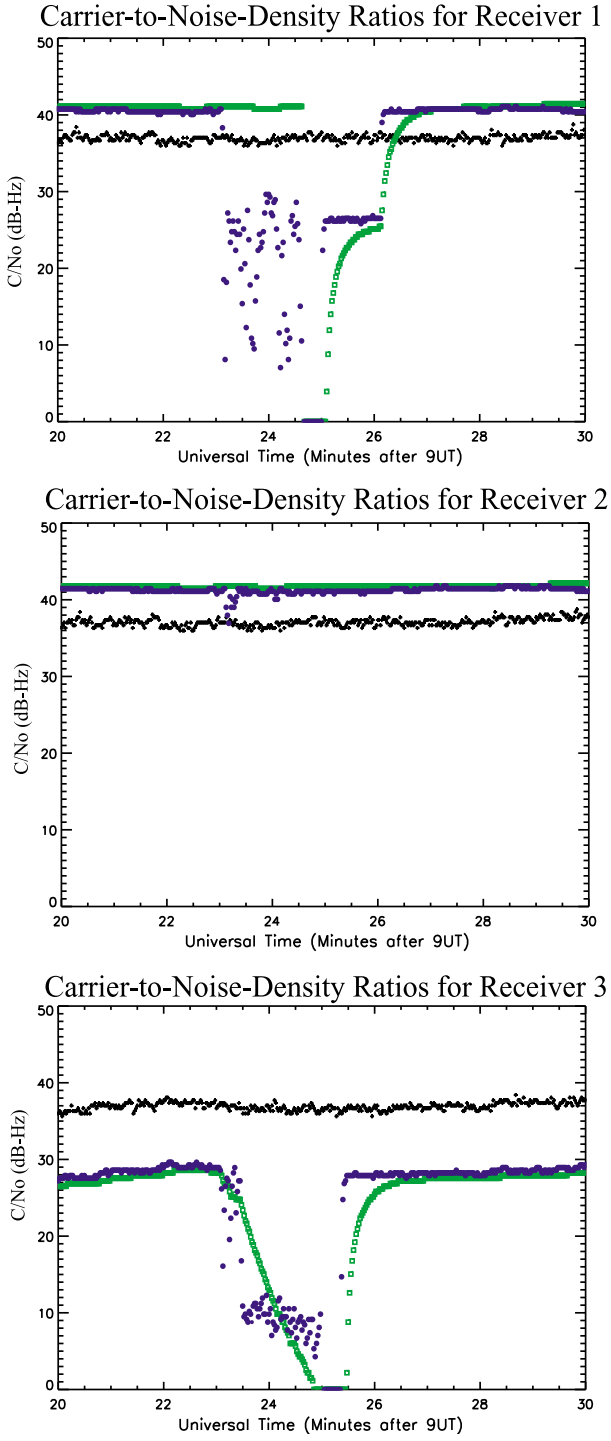

Figure 2. The time series of the carrier-to-noise density ratios (C/No) on each receiver. Receivers 1 and 2 track the full code, while receiver 3 tracks semicodelessly. The C/A C/No is shown as black pluses. The green squares represent the L1 C/No values. The L2 C/No values are presented as blue dots. The scintillation occurred on the first and third receiver's L2 signal.

3.4. Observational Field of View

[17] Figure 4 shows the location of the satellites within the Alaskan station's field of view for a 10 min period from 0920 to 0930 UT. Figure 4 (left) shows the satellite positions as a function of the elevation and azimuth angles, and Figure 4 (right) shows the geographic position of each ray's 100 km pierce point. Because the station is north of the inclination angle of GPS satellites, satellites seen north of the station are transmitting over the pole. During this period, the MSN receivers saw 13 satellites. Seven satellites were below 30° elevation, which is not unusual for high-latitude receivers. The 100 km pierce points are shown because they correspond to altitude of the auroral arc estimated from the airglow spectrum.

[18] The scintillation was observed on the PRN 3 signal, which ranged from 20.35° elevation, 71.87° azimuth at 0923:09 UT to 20.73° elevation, 71.11° azimuth at 0925:01.5 UT. The satellite mainly moved azimuthally (0.76°, compared with −0.38° of elevation) during the event. The corresponding latitudes and longitudes of the 100 km pierce points were 65.30°, 218.01° at 0923:09 UT and 65.32°, 217.90° at 0925:01.5 UT. The receiver field of view during this time period covered a 5.917 km

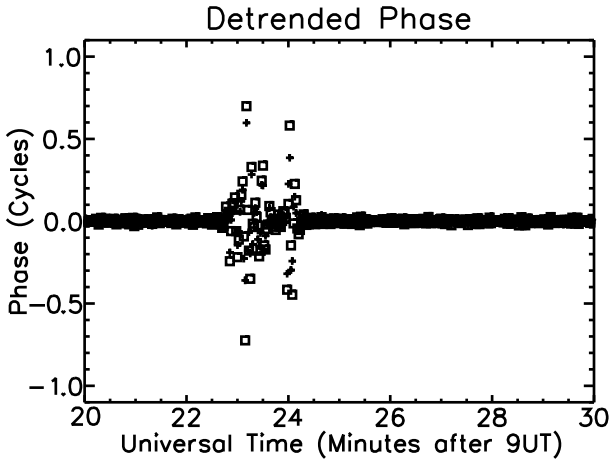

Figure 3. The phase variations in L1 (pluses) and L2 (square) signals during the scintillation event. These phase measurements were taken by receiver 2, which maintained lock during the event, and have been detrended by a sixth-order Butterworth filter and its conjugate.

wide region. Signal loss was not observed on PRN 6, which ranged from 20.67° elevation, 56.95° azimuth (65.83° latitude, 217.43° longitude at 100 km) to 20.93° elevation, 56.18° azimuth (65.84° latitude, 217.34° longitude) over the same time period. The PRN 6 rays were less than 15° of azimuth from the PRN 3 rays. At 100 km, the pierce points were ~65 km apart. Note that both the PRN 3 and PRN 6 rays passed through the auroral arc.

3.5. Ionospheric TEC Observation

[19] Since receiver 2 was able to maintain signal lock through the scintillating region, it was able to observe the ionospheric content associated with the scintillation. Figure 5 shows the slant TEC from the debiased carrier phase differences [*Klobuchar*, 1996; *Garner et al.*, 2008]. The debiasing process removes the phase ambiguities from the TEC calculation, but does not treat the interfrequency biases (which can be as high as 35 TECu (10^{16}/m^2)). These data are presented as line-of-site (LOS) TEC values since the standard obliquity model [*Brunner and Gu*, 1991] assumes a spherical symmetric, thin shell ionosphere. The standard obliquity factor is ~2.2 for this

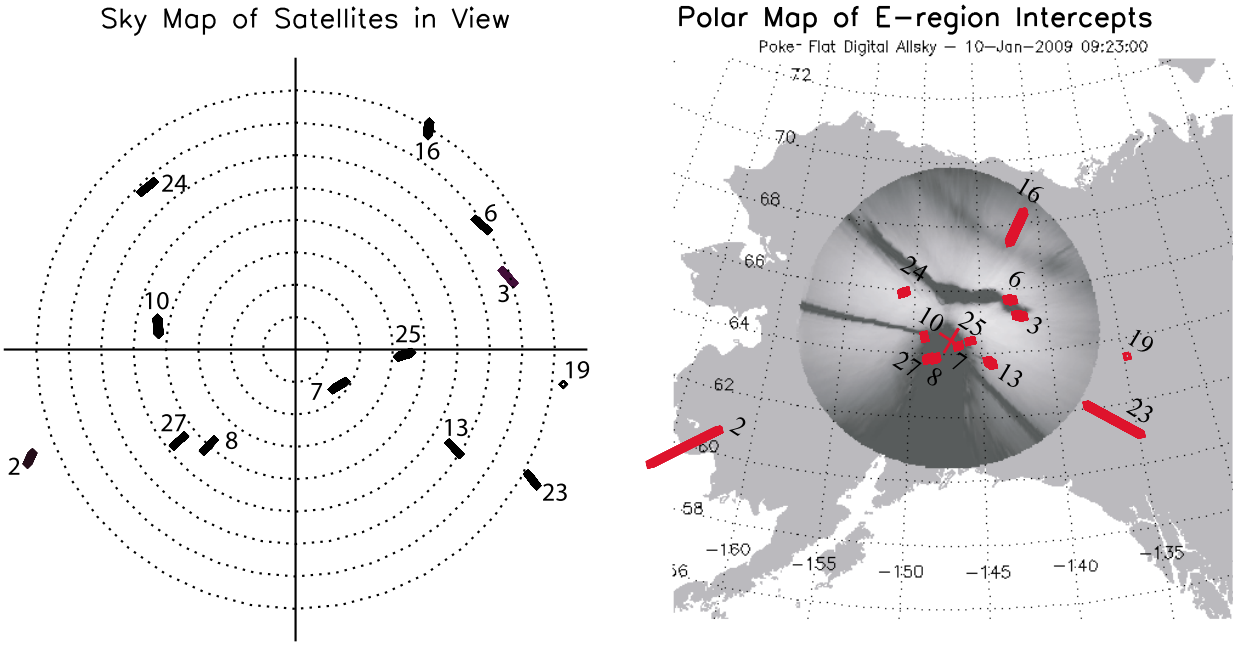

Figure 4. Plots of the Fairbanks station field of view during the scintillation event. (left) An elevation-azimuth map and (right) a map of 100 km pierce points in geographic coordinates. Both maps show the locations of the GPS satellites with each satellite labeled by PRN number. Only 10 min of data are shown from 0920 to 0930 UT. The dashed lines in Figure 4 (left) are lines of constant elevation angles, separated by 10° and starting at 80°. The loss of lock occurred on PRN 3 only.

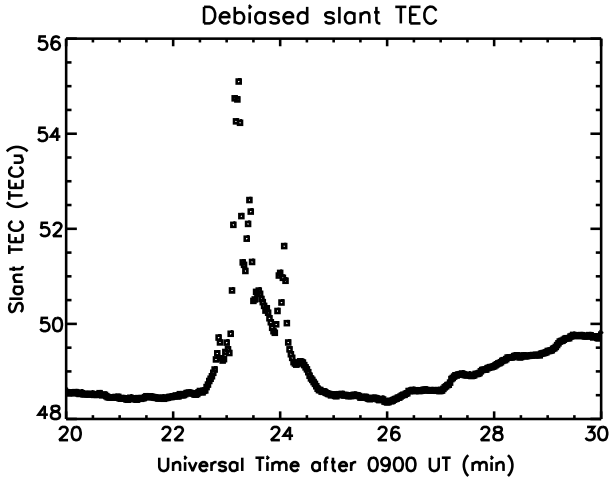

Figure 5. The slant total electron content (TEC) observed by receiver 2 when receivers 1 and 3 lost lock. The TEC is calculated from the phase measurements after the phase ambiguities have been removed. Neither the satellite nor the receiver biases have been removed. The observed plasma structure was 5.71 TECu above the background. The full scintillating region was 5.971 km wide at a 100 km pierce point with a central region that is 523 m across. The TEC gradient in the central region is 10.9 TECu/km if the arc is stationary over this period.

time period, for readers who aim to estimate the vertical TEC.

[20] A substantial TEC gradient existed at 0923 UT. The TEC increased by 5.71 TECu from 0923:03 to 0923:13.5 UT. This corresponds to a distance of 0.523 km and a gradient of 10.9 TECu/km at 100 km if the auroral arc was static over this 10.5 s period. The TEC decreased to a new base line by 0923:30 UT. The scintillation, auroral arc and signal loss were coincident with this sharp gradient. If the TEC increase is converted to vertical using the standard obliquity factor of 2.2 and a simple Chapman layer profile with a 10 km scale height, H, is assumed for the auroral arc, then the peak density of the layer, n_{peak}, would be ~6.28×10^5 cm^{-3}. Here the analytic solution for the Chapman layer TEC ($\sqrt{2\pi e} n_{peak} H$) is used. This peak density is consistent with electron density measurements of auroral arcs [e.g., *de La Beaujardière and Vondrak*, 1982; *Doe et al.*, 1997] and supports *Kintner et al.*'s [2002] assertion that the TEC enhancement within an auroral arc is due to an E region density enhancement.

[21] Figure 6 presents the change in TEC between observations and the corresponding ionosphere-induced phase changes for both the L1 and L2 signals. Figure 6 (top) shows the rate of change in the TEC between observations. This rate was calculated by subtracting the TEC at adjacent time steps and dividing by 1.5 s (the observation cadence). The rate of TEC (ROT) values are placed at the center time between the time steps. The convention is to calculate a rate of TEC index (ROTI) [*Pi et al.*, 1997], which is the standard deviation in the ROT over 5 min. From 0920 to 0925 UT, the ROTI was 5.9584 TECu/min; it was 0.67072 TECu/min for the next 5 min. Figure 6 (bottom) shows the rate of phase change

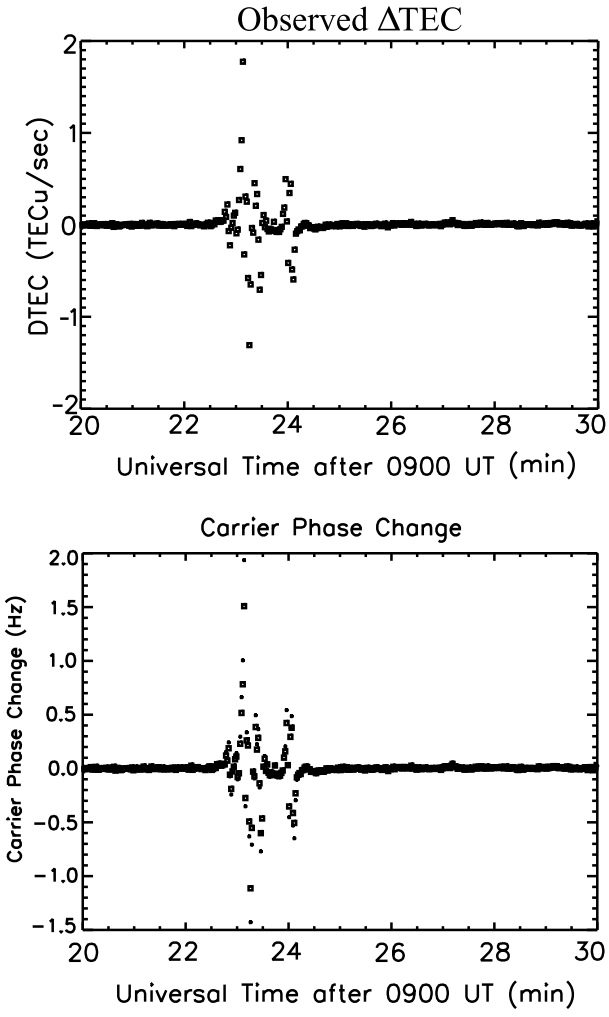

Figure 6. (top) The ROT during the scintillation event and (bottom) the rate of phase change in the L1 (pluses) and L2 (squares). The L2 signals on receivers 1 and 3 were lost a 0923:09 UT when the ROT is ~1.9 TECu/s and the phase change rate was nearly 2 Hz.

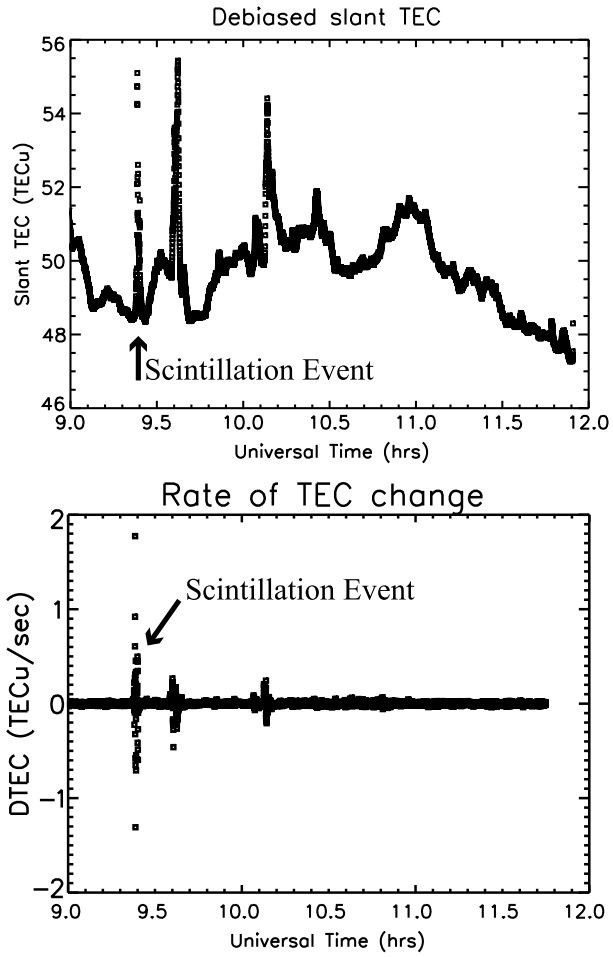

Figure 7. The observed (top) slant [i.e., add space] TEC and (bottom) ROT along the entire PRN 3 overflight. Neither the satellite nor receiver interfrequency bias has been removed. The ionosphere was highly structured with several sharp TEC features. However, only the feature at 0923 UT was associated with a loss of signal lock.

in the both channels over this time period. The rate of phase change was calculated [*Klobuchar*, 1996] from

$$\frac{\Delta\phi}{\Delta t} = \frac{e^2}{8\pi^2\epsilon_0 m_e c f}\frac{\Delta \mathrm{TEC}}{\Delta t} = \frac{1.34\times 10^9 \Delta \mathrm{TEC}}{f\Delta t} \quad (1)$$

where e is the electron charge, ϵ_0 is the permittivity of free space, m_e is the electron mass, c is the speed of light, and f is the signal frequency. Here ϕ is given in cycles, f is in Hz, and TEC is given in TECu (10^{16}/m^2). While equation (1) is a Doppler frequency, it is useful to treat it here as a rate of phase change (RPC). The RPC is integrated over an internal bandwidth within the receiver to produce the phase change to which the tracking loop is exposed. These measurements present a similar picture to the results of Figure 3 but provide a measurement of the phase change free of both satellite geometry and signal filter effects.

[22] There were two other steep TEC gradients that occurred during this satellite pass corresponding to the other two bright arcs seen by the Meridian Scanning Photometer (see Figure 1) later in the hour. These structures are seen in Figure 7. Figure 7 (top) shows the TEC between the receiver and PRN 3 while the satellite is in view. Figure 7 (bottom) shows the corresponding ROT. There were significant ionospheric structures during this time period. However, only the structure at 0923 UT generated a signal loss. This is likely due to the smaller ROT values produced by the TEC gradients at 0938 and 1008 UT. These smaller gradients were observed at slightly later times when PRN6 crossed through this sector. The rays from PRN 6 did not reach the elevation-azimuth angles at which the scintillation occurred, which prevents a comparison of the PRN 3 and PRN 6 behavior to the scintillation event. However, the PRN 6 signal did cross the auroral arc (see Figure 4) when the PRN 3 signal lost lock. Figure 8 shows the LOS TEC from PRN 6 during this period. It shows a weaker TEC gradient than seen by PRN 3, and none of the receivers lost lock. This gradient was observed roughly 12 min after the PRN3 event.

4. Discussion and Conclusion

[23] This paper has addressed a short period of scintillation observed by three collocated high-precision GPS receivers in Fairbanks, Alaska. Two of these receivers share a common antenna and conduct full-code tracking. The third receiver tracks semicodelessly and uses an antenna 62 cm away. This is one of the first publications demonstrating the effects of scintillation on full-code tracking GPS receivers. However, scintillation has been observed previously on full-code tracking receivers (C. Carrano, private communications, 2010).

[24] The intriguing new result from this study is the differing impact ionospheric scintillation had on two nearly identical GPS receivers. The two full-code tracking receivers share a common antenna and are of the same make and model. Both receivers use independent high-precision atomic clock standards. Initially, the L2 C/No values on both receivers decreased. The C/No on one receiver recovered, while the other receiver lost lock. The phase shift caused by the scintillation moved the correlator toward an instability so that one correlator swung back toward the code and the other correlator did not. The correlator that did not swing toward the code lost lock on the signal.

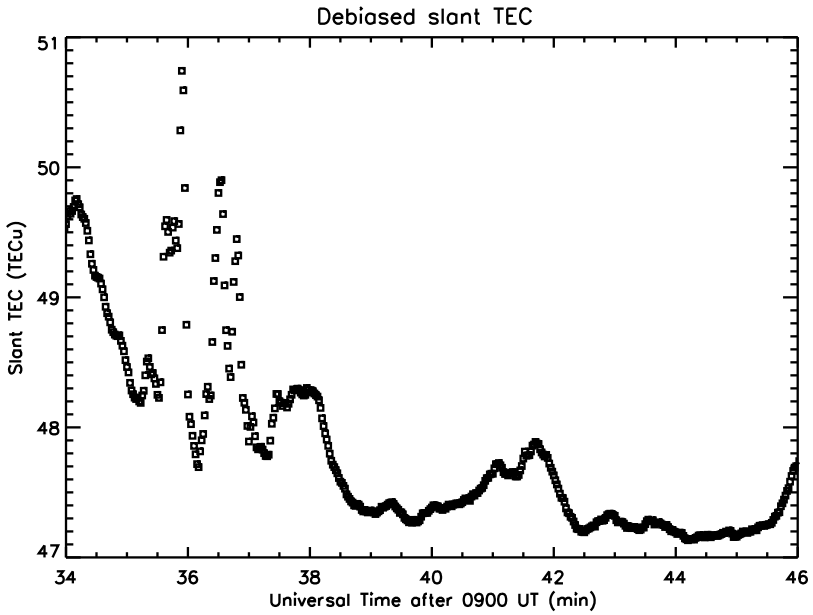

Figure 8. The observed slant TEC from the PRN 6 signal from 0934 to 0946 UT. This time period corresponds to the nearest TEC gradient for the link. Neither the satellite nor receiver interfrequency bias has been removed. Despite the sharp TEC gradient, none of the three receiver lost signal lock.

[25] The observed scintillation occurred on a ray that passed through an auroral arc. While two different rays passed through the auroral arc, signal loss occurred on only one link. No signal disruptions were associated with the subsequent auroral arcs in the GPS receiver's field of view, even though the GPS receivers observed TEC enhancements associated with other arcs. A sharp TEC gradient, estimated at 10.9 TECu/km for E region altitudes and a stationary arc, was observed in the arc. The corresponding E region density peak increase was ~6.28×10^5 cm^{-3}, which is reasonable for auroral precipitation. The GPS ray was within the arc for 78 s, which corresponds to 5.91 km if the arc is stationary.

[26] The observations reported here demonstrate the complexity of a GPS receiver's response to the plasma irregularities within an auroral arc. While the auroral arc remains within the receiver's field of view for tens of minutes, the scintillation event only lasted 78 s and only affected only one satellite link. It caused a degradation that made the L2 signal loose lock. The L1 signal did not. The most likely cause for the loss of the L2 signal, but not L1 or C/A signals, is that the maximum received L2 power is 2.5 dBW lower than the L1 power for the present generation of GPS satellites [*GPS Joint Program Office*, 2006]. The longer wavelength of the L2 signal may also contribute since scintillation is a function of λ/D where D is the scale length of the plasma irregularity. After GPS modernization has been completed, the both signals will transmit at the same power level. The increased power levels and the use of the civilian codes will likely improve a GPS receivers response to scintillation, but neither are guaranteed to solve the scintillation problem. That two identical, zero baseline receivers reacted differently to ionospheric scintillation indicates that a receiver's internal state partially determines the impact of scintillation on its performance. Improved transmission power and civilian codes are not enough to solve the ionospheric scintillation problem. However, the development of multiple independent correlators within a single receiver (essentially multiple receivers) may also reduce the impact of scintillation. Any engineering solution to ionospheric scintillation will require improved receiver hardware and more advanced signal correlators.

[27] **Acknowledgments.** This work was supported at the Applied Research Laboratories, University of Texas at Austin, by the National Geospatial-Intelligence Agency under the contract NGA-6200-5-36. The authors wish to thank Charles Carrano, Paul Kintner, Keith Wyborny, and Ann Brunham for their useful input and insightful comments.

References

Aarons, J. (1982), Global morphology of ionospheric scintillations, *Proc. IEEE*, *70*, 360–172.

Basu, S. (1975), Universal time seasonal variation of auroral zone magnetic activity and VHF scintillation, *J. Geophys. Res.*, *80*, 4725–4728.

Basu, S., and J. Aarons (1980), The morphology of high-latitude VHF scintillation near 70°W, *Radio Sci.*, *15*, 59–70.

Basu, S., and S. Basu (1981), Equatorial scintillations—A review, *J. Atmos. Terr. Phys.*, *43*, 473–489.

Basu, S., et al. (1996), Scintillations, plasma drifts, and neutral wind in the equatorial ionosphere after sunset, *J. Geophys. Res.*, *101*, 26,795–26,809.

Brunner, F. K., and M. Gu (1991), An improved model for the dual frequency ionospheric correction of GPS observations, *Manuscr. Geod.*, *16*, 205–214.

Coker, C., G. S. Bust, R. A. Doe, and T. L. Gaussiran II (2004), High-latitude plasma structure and scintillation, *Radio Sci.*, *39*, RS1S15, doi:10.1029/2002RS002833.

Coster, A., S. Skone, C. Mitchell, G. D. Franceschi, L. Alfonso, and V. Romano (2005), Global studies of GPS scintillation, paper presented at Institute of Navigation National Technical Meeting 2005, Inst. of Navigat., Inc., San Diego, Calif.

Creel, T., A. J. Dorsey, P. J. Mendicki, J. Little, R. G. Mach, and B. A. Renfro (2007), Summary of accuracy improvements from the GPS legacy accuracy improvement initiative (L = AII), paper presented at GNSS 20th International Technical Meeting, Sat. Div., Inst. of Navigat., Fort Worth, Tex.

Davies, K. (1990), *Ionospheric Radio*, Peter Peregrinus, London.

de La Beaujardière, O., and R. Vondrak (1982), Chatanika radar observations of the electrostatic potential distribution of an auroral arc, *J. Geophys. Res.*, *87*, 797–809.

Doe, R. A., J. D. Kelly, D. Lummerzheim, G. K. Parks, M. J. Brittnacher, G. A. Germany, and J. Spann (1997), Initial comparison of Polar UVI and Sondrestrom IS radar estimates for auroral electron energy flux, *Geophys. Res. Lett.*, *24*, 999–1002.

Doherty, P. H., S. H. Delay, C. E. Valladares, and J. A. Klobuchar (2003), Ionospheric scintillation effects in the equatorial and auroral regions, *Navigation*, *50*, 235.

Fejer, B. G., L. Scherliess, and E. R. dePaula (1999), Effects of the vertical plasma drift velocity on the generation and evolution of equatorial spread *F*, *J. Geophys. Res.*, *104*, 19,859–19,870.

Forte, B. (2008), Refractive scattering evidence from multifrequency scintillation spectra observed at auroral latitudes, *Radio Sci.*, *43*, RS2012, doi:10.1029/2007RS003715.

Forte, B., and S. M. Radicella (2002), Problems in data treatment for ionospheric scintillation measurements, *Radio Sci.*, *37*(6), 1096, doi:10.1029/2001RS002508.

Garner, T. W., T. L. Gaussiran II, B. W. Tolman, R. B. Harris, R. S. Calfas, and H. Gallagher (2008), Total electron content measurements in ionospheric physics, *Adv. Space Res.*, *42*, 720–726.

GPS Joint Program Office (2006), Navstar GPS space segement/navigation user interfaces, Interface specification IS-GPS-200, *Tech. Rep. IRN-200D-001*, Space and Missile Syst. Cent., El Segundo, Calif.

Groves, K. M., S. Basu, J. M. Quinn, T. R. Pedersen, K. Falinski, A. Brown, R. Silva, and P. Ning (2000), A comparison of GPS performance in a scintillation environment at Ascension Island, paper presented at ION-GPS 2000, Inst. of Navigat., Inc., Salt Lake City, Utah.

Jayachandran, P. T., K. Hosokawa, J. W. MacDougall, S. Mushini, R. B. Langley, and K. Shiokawa (2009), GPS total electron content variations associated with a polar cap arc, *J. Geophys. Res.*, *114*, A12304, doi:10.1029/2009JA014916.

Kintner, P. M., H. Kil, C. Deehr, and P. Schuck (2002), Simultaneous total electron content and all-sky camera measurements of an auroral arc, *J. Geophys. Res.*, *107*(A7), 1127, doi:10.1029/2001JA000110.

Kintner, P. M., B. M. Ledvina, and E. R. de Paula (2007), GPS and ionospheric scintillations, *Space Weather*, *5*, S09003, doi:10.1029/2006SW000260.

Klobuchar, J. A. (1996), Ionospheric effects on GPS, in *Global Positioning System: Theory and Applications*, edited by B. W. P. and J. J. Spikler Jr., p. 485, Am. Inst. of Aeronaut. and Astronaut., Inc., Washington D. C.

Martin, E., and J. Aarons (1977), F layer scintillations and the aurora, *J. Geophys. Res.*, *82*(19), 2717–2722.

Nichols, S., A. Hansen, T. Walter, and P. Enge (2000), High-latitude measurements of ionospheric scintillation using the NSTB, *Navigation*, *47*, 112.

Pi, X., A. J. Mannucci, U. J. Lindqwister, and C. M. Ho (1997), Monitoring of global ionospheric irregularities using the Worldwide GPS Network, *Geophys. Res. Lett.*, *24*(18), 2283–2286.

Pryse, S. E., L. Kersley, and I. K. Walker (1996), Blobs and irregularities in the auroral ionosphere, *J. Atmos. Terr. Phys.*, *58*, 205–215.

Rees, M., and D. Luckey (1974), Auroral electron energy derived from ratio of spactroscopic emmisions: 1. Model computation, *J. Geophys. Res.*, *79*, 5181–5186.

Rino, C. L. (1979), A power law phase screen model for ionospheric scintillation: 1. Weak scatter, *Radio Sci.*, *6*, 1135–1145.

Rino, C. L., and S. J. Matthews (1980), On the morphology of auroral zone radio wave scintillation, *J. Geophys. Res.*, *85*, 4139–4151.

Smith, A. M., C. N. Mitchell, R. J. Watson, R. W. Meggs, P. M. Kintner, K. Kauristie, and F. Honary (2008), GPS scintillation in the high arctic associated with an auroral arc, *Space Weather*, *6*, S03D01, doi:10.1029/2007SW000349.

Su, S.-Y., C. K. Chao, and C. H. Liu (2008), On monthly/seasonal/longitudinal variations of equatorial irregularity occurrences and their relationship with the postsunset vertical drift velocities, *J. Geophys. Res.*, *113*, A05307, doi:10.1029/2007JA012809.

Tsunoda, R. T. (1988), High-latitude F region irregularities: A review and synthesis, *Rev. Geophys.*, *26*(4), 719–760.

Yeh, K. C., and C.-H. Liu (1982), Radio wave scintillations in the ionosphere, *Proc. IEEE*, *70*, 324–360.

T. W. Garner, R. B. Harris, and J. A. York, Signal and Geophysics Laboratory, Applied Research Laboratories,

University of Texas, PO Box 8029, Austin, TX 78758-4423, USA. (garner@arlut.utexas.edu; pben@arlut.utexas.edu; york@arlut.utexas.edu)

D. L. Hampton, Geophysical Institute, University of Alaska Fairbanks, Fairbanks, AK 99775-7320, USA. (dhampton@gi.alaska.edu)

C. S. Herbster and C. F. Minter, National Geospatial-Intelligence Agency, Mail Stop L-22, 3838 Vogel Rd., Arnold, MO 63010-6238, USA. (Chris.S.Herbster@nga.mil; Clifton.F.Minter@nga.mil)